Location of trivalent lanthanide dopant energy levels in (Lu0.5Gd0.5)2O3

H. Rétot, A. Bessière, B. Viana, and A. Galtayries

Citation: Journal of Applied Physics **109**, 123518 (2011); doi: 10.1063/1.3597788
View online: http://dx.doi.org/10.1063/1.3597788
View Table of Contents: http://scitation.aip.org/content/aip/journal/jap/109/12?ver=pdfcov
Published by the AIP Publishing

Location of trivalent lanthanide dopant energy levels in $(Lu_{0.5}Gd_{0.5})_2O_3$

H. Rétot,[1] A. Bessière,[1,2,a)] B. Viana,[1] and A. Galtayries[3]
[1]*Chimie Paristech, Laboratoire de Chimie Matière Condensée de Paris, UPMC, Collège de France, UMR - CNRS 7574, 11 rue Pierre et Marie Curie, 75231 Paris Cedex 05, France*
[2]*Department of Physics, Goa University, Taleigao Plateau, Goa 403 206, India*
[3]*Chimie Paristech, Laboratoire de Physico-Chimie des Surfaces, UMR - CNRS 7045, 11 rue Pierre et Marie Curie, 75231 Paris Cedex 05, France*

(Received 12 January 2011; accepted 10 May 2011; published online 22 June 2011)

The location of Ln^{3+} dopant energy levels relative to bands in $(Lu_{0.5}Gd_{0.5})_2O_3$ was studied. A several-steps analysis of XPS measurements on heavy lanthanides sesquioxides Ln_2O_3 (Ln = Gd, Tb, Dy, Er, Tm, Yb, Lu) and on Sc_2O_3 and Y_2O_3 reference materials were used to locate Ln^{3+} dopant ground state relative to the top of the valence band in $(Lu_{0.5}Gd_{0.5})_2O_3$ within an error bar of ±0.4 eV. The agreement between XPS data and model was found improved relative to previous studies. When compared to XPS analysis, prediction based on optical absorption shows a slight underestimation attributed to the lack of precision in Ce^{4+} charge transfer band measurement.
 [doi:10.1063/1.3597788]

I. INTRODUCTION

Many performances of optical materials are determined by the location of lanthanide energy levels relative to the conduction and valence bands of the matrix. Elaboration of a full energy diagram can be very useful for applications such as phosphors, scintillators or solid-state lasers, as it allows a better understanding of the optical behavior. By compiling the enormous amount of experimental data based on absorption, excitation and emission spectra reported in the literature, Dorenbos developed predicting tools to locate the fundamental $4f^n$ state and the lowest $4f^{n-1}5d^1$ excited level of trivalent (Ln^{3+}) and divalent (Ln^{2+}) lanthanides dopants relative to the bands of the host crystal. In his first studies on the subject, he showed that provided the $4f^n \rightarrow 4f^{n-1}5d^1$ transition energy is known for one Ln^{3+}, the $4f^n \rightarrow 4f^{n-1}5d^1$ transition energies for all the other Ln^{3+} of the series can be predicted since the difference between the $4f^n \rightarrow 4f^{n-1}5d^1$ energies of any two Ln^{3+} was found constant in a large number of halogenides and chalcogenides.[1–3] These constant values were given as the averaged experimental values recorded over more than three hundreds compounds, giving a strong support to the predictive tool. The same review on $4f^n \rightarrow 4f^{n-1}5d^1$ energies was carried out for divalent lanthanide ions.[4] The next important step was to locate the fundamental $4f^n$ state and/or the lowest $4f^{n-1}5d^1$ excited level relatively to the bands of the crystal host. The knowledge of this location is of high interest in the field of luminescent materials as many properties depend on the location of the dopant states inside the forbidden gap of the host. The ability of lanthanide ions to trap a hole from the valence band or an electron from the conduction band for example is related to the location of energy levels relative to host levels, which can determine phosphors efficiency.[5,6] Likewise, the location of the dopant states in a laser crystal explains excited state absorption and auto-ionization which lead to loss mechanisms.[7] In scintillators, the position of the $4f^{n-1}5d^1$ level can explain a low light yield hampered by auto-ionization.[8–11] In persistent phosphors, the position of the $4f^{n-1}5d^1$ level relative to the conduction band determines whether or not a delocalization process is possible. When the lanthanide ion acts as a trap, the location of its fundamental $4f^n$ level determines the trap depth and hence the intensity and the duration of the persistent phosphorescence at a given temperature.[12–14] Likewise, the position of the $4f^n$ states is important for neutron detectors[15] and x-ray storage phosphors.[16]

To achieve the goal of locating lanthanide ions levels relative to the bands of the host, several paths were followed. Studies were conducted on divalent lanthanides. On the one hand, theoretical arguments taking into account (i) the change in the Madelung potential due to lattice relaxation, (ii) the Coulomb interaction between the 5d electron and the lanthanide ion, and (iii) the isotropic exchange interaction between the 5d electron spin and the total spin of the $4f^{n-1}$ electrons were considered to locate semiquantitatively the lowest $4f^{n-1}5d^1$ excited level relative to the bottom of the conduction band in CaF_2, SrF_2, and BaF_2. The location of the levels then explains the anomalous emission of Eu^{2+} and Yb^{2+} observed in some compounds.[17] On the other hand by compiling experimental data on charge transfer (CT) energies of Ln^{3+}, Dorenbos showed that the energy difference between the top of the valence band and the fundamental $4f^n$ state of Ln^{2+} can be predicted for any lanthanide provided the value is known for one Ln^{2+}.[18] Up-to-date prediction was recently published.[19] Coupling the results with the $4f^n \rightarrow 4f^{n-1}5d^1$ transition energies, an absolute energy location of the lowest $4f^{n-1}5d^1$ of Ln^{2+} was determined, which was found slightly different from the one obtained by theoretical arguments in Ref. 17.

In order to provide information for trivalent lanthanides, one would need the same amount of data on CT energies for Ln^{4+} than for Ln^{3+}. However, data on CT in Ln^{4+}-doped compounds are scarce and it was not possible to gather enough experimental data to ascertain a model for Ln^{3+}.

a)Electronic mail: aurelie-bessiere@chimie-paristech.fr.

Instead arguments developed in Refs. 17, 18, and 20 were used to predict that the energy of the $4f^{n-1}5d^1$ levels for Ln^{3+} should vary along the lanthanides series in a way similar to Ln^{2+} weighed by a coefficient of 1.2, to correct for lattice relaxation, Coulomb interaction between the 5d and the $4f^{n-1}$ electrons and isotropic exchange interaction between the 5d electron spin and the total spin of the $4f^{n-1}$ electrons. Then coupling the position of the Ln^{2+} $4f^{n-1}5d^1$ states with the $4f^n \rightarrow 4f^{n-1}5d^1$ transition energies enables one to locate the fundamental $4f^n$ states of Ln^{2+}. Hence, a predictive model is also available for trivalent lanthanides location, but it does not yet appear as much supported by experimental evidence as for divalent lanthanides due to the lack of optical experimental data.

In this paper, we propose to provide experimental data on Ln^{3+} $4f^n$ fundamental state location by using x-ray photoelectron spectroscopy (XPS). Photoelectron spectroscopy as a tool to locate lanthanides energy levels was popularized by Thiel *et al.*[21,22] and used by several others.[5,23,24] It is based on the measurement of the binding energies of electrons of the lanthanide as well as of the valence band, making possible a direct comparison of energies. However, just like several other experimental methods used to locate dopant energy levels in a host crystal (photoconductivity, excited-state absorption for instance) signals are often broadened and one needs to carefully examine the data in order to extract valuable information. In this paper, XPS data recorded on M_2O_3 sesquioxides with M = Sc, Y, Gd, Tb, Dy, Er, Tm, Yb, Lu were studied with the aim of (i) locating experimentally the energy levels of the heavy trivalent lanthanides Ln^{3+} (Ln = Gd, Tb, Dy, Er, Tm, Yb) as dopants relative to the bands of $(Lu_{0.5}Gd_{0.5})_2O_3$ host, (ii) discussing the XPS data in relationship with model predictions, and (iii) discussing the scintillation potential of Ln^{3+} doping in $(Lu_{0.5}Gd_{0.5})_2O_3$ from the energy scheme of Ln^{3+}.

Lu_2O_3 is a material of choice in scintillation as it presents very high stopping power due to high density ($\rho = 9.43$ g/cm^3) and large effective atomic number ($Z_{eff} = 69$). It presents a cubic crystal structure (bixbyite) with space group Ia-3 (206). Two distinct cationic sites with symmetry C_2 (non centrosymmetric) and S_6 (centrosymmetric) exist in a ratio 3:1. The two sites are available to lanthanide doping by substitution of Lu^{3+} and were shown to present distinct scintillation properties when occupied by Eu^{3+}.[25] $(Lu_{0.5}Gd_{0.5})_2O_3$ presents the same bixbyite structure as Lu_2O_3 while the introduction of gadolinium enlarges the lattice parameters. The cationic sites therefore accommodate Ln^{3+} dopants with less strain and show a different distribution of Ln^{3+} dopants between both sites.[26] This last property was shown to favorably influence the scintillation properties[26] which justifies our interest for this mixed oxide.

II. EXPERIMENTAL

M_2O_3 with M = Sc, Y, Gd, Tb, Dy, Er, Tm, Yb, Lu as well as $(Lu_{0.5}Gd_{0.5})_2O_3$ were prepared by a coprecipitation method. M nitrates were dissolved in de-ionized water and added dropwise into an ammonia and oxalic acid solution with pH = 9 while stirring. A white precipitate was obtained. It was washed with water and then ethanol before being dried at 100 °C. The powder was then fired at 1000 °C. The purity of the phase was checked by x-ray diffraction and all compounds were found perfectly pure.

XPS measurements were performed with an ESCALAB 250 spectrometer (Thermo Electron Corporation) using a monochromatized, focused Al K_α x-ray source ($h\nu = 1486.6$ eV). The sample powders were deposited on a double sided tape and a 2 V flood gun was used during all time of the analysis. The analysis area was a spot of about 500 μms diameter.

A survey spectrum was systematically recorded with a pass energy of 100 eV (step energy: 1 eV). From the examination of this spectrum, the core level regions of interest were defined (O 1s, C 1s as well as the core level of the lanthanide cations, such as Ln 4f) as well as the region of the valence band (XPS VB) and have been recorded at high resolution (pass energy of 20 eV, step energy: 0.1 eV) with a take-off angle of 90°. The spectrometer was calibrated against the reference binding energies (BEs) of clean Cu (932.6 eV), Ag (368.2 eV), and Au (84.0 eV) samples. Though a charge compensation system was used during the analysis (flood gun), the question of the binding energy correction and differential charging effects (between compounds) was raised. We chose either to quote "as read" uncorrected binding energies or to use the Sc_2O_3 compound as a reference compound and a constant energy difference between the binding energies of the O 1s and O 2p levels. This will be explicitly developed in the following. The experimental binding energies are given with an accuracy of 0.2 eV.

III. RESULTS AND DISCUSSION

A. Binding energies determined by XPS

As XPS enables to measure binding energies of 4*f* electrons in lanthanides, one can expect information about the difference in energy between the $4f^n$ levels of a lanthanide introduced as dopant in a material and the valence band. In order to locate the energy levels of Ln^{3+} dopant relatively to the valence band of the host, here the mixed lutetium-gadolinium oxide $(Lu_{0.5}Gd_{0.5})_2O_3$, we have to consider the energy difference between the states constituting the top of the valence band and the fundamental $4f^n$ state of Ln^{3+} dopant. To do so, we assumed that cubic M_2O_3 with M = Sc, Y, Gd, Tb, Dy, Er, Tm, Yb, Lu as well as $(Lu_{0.5}Gd_{0.5})_2O_3$ compounds have similar band structures. In Y_2O_3 it was shown that the top of the valence band was mainly constituted by O 2p states.[27] We therefore considered that the energy difference between the O 2p and the $4f^n$ states of the Ln^{3+} dopant represents the location of the fundamental state of Ln^{3+} dopant relative to the valence band of $(Lu_{0.5}Gd_{0.5})_2O_3$.

Preliminary XPS measurements were recorded on $(Lu_{0.5}Gd_{0.5})_2O_3$: x % Ln^{3+} with $x < 10\%$ to tentatively observe the $4f^n$ electronic states of both Ln^{3+} dopant and Lu^{3+} and Gd^{3+} host ions as well as the valence band of $(Lu_{0.5}Gd_{0.5})_2O_3$ on the same spectrum allowing the energies to be measured relative to a common reference. However, as the amount of Ln^{3+} was much lower than the one of oxygen, lutetium, and gadolinium, the signal of the $4f^n$ states of Ln^{3+} dopants could not be clearly observed neither in the XPS VB

nor in core levels. Therefore, we made the assumption that the $4f^n$ energy states are located at the same energy for Ln^{3+} as dopant in $(Lu_{0.5}Gd_{0.5})_2O_3$ as for Ln^{3+} as the main cation in any corresponding Ln_2O_3. As 4f electrons are very much shielded from their environment by outer 5s and 5p electrons, they present limited interaction and their energy should be close to the energy of isolated Ln^{3+} dopants in a similar host material. This was experimentally verified by Thiel *et al.* in $Y_3Al_5O_{12}$:Ln^{3+} (Ln = Gd, Tb, Dy, Ho, Er, Tm, Yb, Lu). No shift in binding energies within the experimental accuracy of several meV was observed between the 7% and 100% Gd^{3+}-doped compounds or between the 10% and 100% Yb^{3+}-doped compounds.[21] Bouttet *et al.* also reported that no variation in the valence band shape and no shift in the Ce 4f states was observed moving from LaF_3: 10% Ce^{3+} to CeF_3.[28] Therefore in this work, we decided to record x-ray photoelectron spectra of Ln_2O_3 with Ln = Gd, Tb, Dy, Er, Tm, Yb, Lu for getting information on Ln^{3+}-doped $(Lu_{0.5}Gd_{0.5})_2O_3$. One can notice that all the considered M_2O_3 compounds (M = Sc, Y, Gd, Tb, Dy, Er, Tm, Yb, Lu) have the same cubic bixbyite (Ia-3) structure as Lu_2O_3 and that in addition, the XPS VB spectrum (not presented here) of the mixed $(Lu_{0.5}Gd_{0.5})_2O_3$ is composed of the superposition of the Gd_2O_3 and Lu_2O_3 XPS spectra.

Figure 1 shows the experimental x-ray photoemission spectra of the compound Lu_2O_3 (a) together with the ones of Y_2O_3, (b) and Sc_2O_3, (c) over the 0–40 eV (XPS VB) and the 522–538 eV (O 1s core level) ranges. Let us first consider the XPS VB. For Lu_2O_3, signals at 31.8 and 25.4 eV are attributed to Lu $5p_{1/2}$ and $5p_{3/2}$ core levels, respectively.[29] O 2s electrons are observed at about 18 eV. The Lu 4f core level is observed between 10 and 4 eV while O 2p lies at about 4 eV. A minimum of two components can be observed in the Lu 4f core level. The Lu 4f core level was fitted by Gaussian/Lorentzian curves as shown in Fig. 1, using a Shirley background, full widths at half maximum (FWHM) of 1.7 ± 0.1 eV, an energy splitting of 1.1 ± 0.1 eV and an intensity ratio of $(2\ J_{5/2}+1)/(2\ J_{7/2}+1) = 0.75$. However, the relative intensities of the two components of the peak do not correspond well to the ratio of the respective degeneracies of the Lu $4f_{5/2}$-Lu $4f_{7/2}$ spin-orbit doublet represented by the fitting curve. This suggests that at least two different Lu 4f doublets may be present in the spectrum. The same conclusion was drawn by Perego *et al.*[30] in the analysis of 3 to 10 nm-thick Lu_2O_3 films. Similarly to their work, we can suggest the presence of both Lu_2O_3 and $Lu(OH)_3$, as also supported by the analysis of the O 1s core level which presents at least two features (see further). $Lu(OH)_3$ is indeed expected as Lu_2O_3 is a highly hygroscopic material. Assuming a small error due to the two species Lu_2O_3 and $Lu(OH)_3$ and based on the Lu 4f peak decomposition, (uncorrected) binding energies of 5.4 and 6.5 eV were found for the Lu $4f_{5/2}$ and $4f_{7/2}$ peaks respectively in Lu_2O_3.

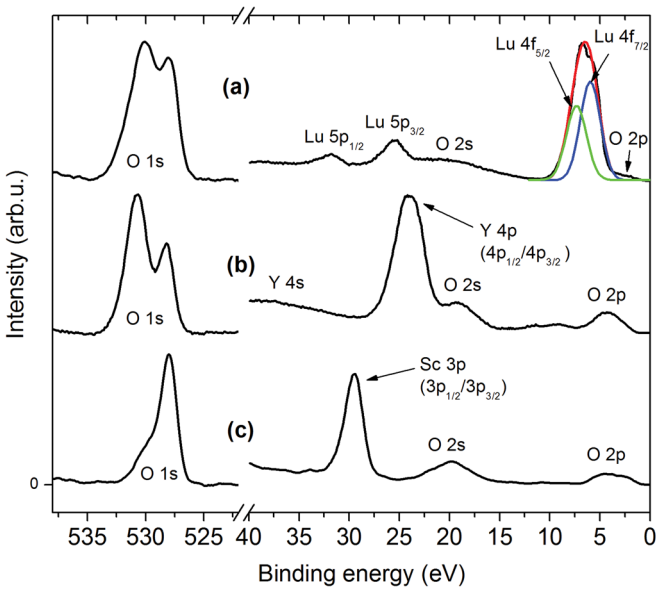

FIG. 1. (Color online) X-ray photoelectron spectra of the XPS VB (valence band) and the O 1s core level of (a) Lu_2O_3, (b) Y_2O_3, (c) Sc_2O_3.

Because of the partial overlapping of these peaks with the weaker O 2p signal in Lu_2O_3, it appeared difficult to determine the binding energy of O 2p with sufficient accuracy. In Y_2O_3 and Sc_2O_3 spectra, the signals attributed to yttrium and scandium are indicated on the figure at energies above 20 eV. O 2s states are located at around 19 eV while O 2p signals are nicely separated from the rest of the spectra in the 2–7 eV range. This enabled us to locate the maximum of the O 2p peaks at 4.3 and 4.0 eV for Y_2O_3 and Sc_2O_3, respectively.

O 1s core levels were observed within the 522–538 eV energy range, without any overlapping with any signal from Auger lines or core levels. For Sc_2O_3 the O 1s binding energy is located at 527.9 eV. For Y_2O_3 two peaks are observed corresponding on the one hand to the signal of oxygen in oxide (bulk contribution) and on the other hand to the signal of oxygen originating from hydroxyl groups or organic contamination (surface contribution). The lower binding energy peak is attributed to the bulk sesquioxide whereas the higher binding energy peak is attributed to oxygen from surface contamination. Thus, the O 1s binding energy was found at 528.2 eV in Y_2O_3. O 1s is expected to show the same binding energy in Sc_2O_3 as in Y_2O_3. The small shift (0.3 eV) observed between the O 1s peaks is therefore an evidence of differential charging effects between samples. Hence, we chose to take Sc_2O_3 as the reference and corrected the BEs of O 2p in Y_2O_3 with a correction shift of $BE_{corr} = 4.3 - (528.2–527.9) = 4.0$ eV.

Sc_2O_3 and Y_2O_3 are often considered along with the lanthanide sesquioxide series as they display the same bixbyite structure as cubic Ln_2O_3 and similar chemical properties.[31] On the one hand, the ionic radius (r_i) of 6-coordinated Y^{3+} is 0.892 Å. It is therefore very close to r_i (VI-Er^{3+}) = 0.89 Å[32] which implies similar lattice parameter and metal oxygen bond strengths for Y_2O_3 and Er_2O_3. On the other hand, r_i (VI-Sc^{3+}) = 0.730 Å is slightly shorter than the smallest ionic radius of the trivalent lanthanide series r_i (VI-Lu^{3+}) = 0.86 Å. Hence a variation of the lattice parameter from 9.8 Å to 10.4 Å is observed between Sc_2O_3 and Lu_2O_3 implying longer bond lengths for Lu_2O_3. We found that the correcting shifts of O 2p for Sc_2O_3 and of O 2p for Y_2O_3 were both equal to 4.0 eV. As the difference in bond strengths between Y_2O_3 and any Ln_2O_3 or in between Ln_2O_3 with Ln = Gd, Tb, Dy, Er, Tm, Yb, Lu will anyway be

smaller than between Y_2O_3 and Sc_2O_3, we can assume that no significant shift of O 2p binding energy should be observed between Y_2O_3 and any Ln_2O_3 as well as along the Ln_2O_3 series (Ln = Gd, Tb, Dy, Er, Tm, Yb, Lu). Therefore, in the following we used this constant value of BE(O 1s, oxygen of the bulk oxide) – BE(O 2p) $= \Delta BE = 523.9$ eV measured for Y_2O_3 and for Sc_2O_3 to find the corrected binding energy of O 2p in all the considered Ln_2O_3 compounds. Indeed, in most of the Ln_2O_3 compounds, the O 2p peak is hidden by the Ln 4f level since the photoionization cross section of the O 2p state is 0.1405 with a photon energy of 1486.6 eV whereas for the O 1s peak, the photoemission cross-section is reported to be 2.93 with the same photon energy.[33] Thus, we systematically used the O 1s core level peak and the constant ΔBE value determined with Sc_2O_3 to calculate the position of the O 2p state with a satisfactory accuracy. For instance, with Lu_2O_3, the O 2p state was found, after correction, located at 4.1 eV (= 528.0–523.9).

Figure 2 shows the O 1s core level spectra of all the Ln_2O_3. Similarly to Y_2O_3 spectrum in Fig. 1, the Ln_2O_3 spectra are composed of two contributions of variable intensity and distant of about 2.5 eV. As described above, we considered for Y_2O_3 that the lowest BE peak was related to the oxygen in bulk Ln_2O_3. The maxima of these peaks are indicated in Fig. 2 as black triangles and their values are reported in Table I. An error bar of ± 0.2 eV due to the determination of the peak maximum should be taken into account. The BEs of O 2p (obtained by subtracting 523.9 eV to the low BE contribution of the O 1s core level) are reported in Table I for each Ln_2O_3.

Figure 3 displays the Ln 4f core level spectra of all Ln_2O_3. The abscissa of all the spectra have been shifted so that the maxima of the O 2p peaks, reported in Table I for every Ln_2O_3, appear all at 4.0 eV on the figure, i.e., along the vertical dash line in Fig. 3. In order to extract the binding energies of the 4f electrons, one needs to consider the multiplet splitting of the final state. Once a 4f electron has been ejected, Ln^{3+} becomes Ln^{4+} (final state) which can be left in various excited and ground states. For a given Ln^{3+} with a $4f^n$ configuration, the possible states of Ln^{4+} are similar to the excited state of Ln^{3+} with $4f^{n-1}$ configuration. For instance, the final state for the 4f electrons of Dy^{3+} will be ^7F_J (J = 6, 5, 4, 3, 2, 1, 0), $^5D_4$…etc. These configurations correspond to levels of Dy^{4+} or Tb^{3+} reported on Dieke diagrams. The energy differences between the multiplet levels given by Dieke diagram were corrected for the charge difference from 3+ to 4+. The energy differences can be considered as 10% larger for Ln^{4+} than for Ln^{3+} with the same $4f^{n-1}$ electronic configuration.[21] The Ln^{3+} to Ln^{4+} levels transition probabilities were calculated by Cox.[34] Hence the lowest BE part of each spectrum was fitted by a set of Gaussians with fixed relative intensities and fixed relative peak position as indicated by bars on Fig. 3. The FWHM was an adjustable parameter but was kept identical for every peak of the same Gaussian set. As the 4f BE is given by the value of the fundamental final state, we focused our study on this lowest 4f BE in the multiplet. In this energy range, O 2p states are present but we neglected their influence due to to their very low intensity.

For Lu_2O_3, the Lu 4f multiplet is composed of $4f_{5/2}$ and $4f_{7/2}$ levels of Lu^{4+} as displayed by two bars in Fig. 3. The

TABLE I. As-measured O 1s binding energy (BE) and calculated O 2p BE in Ln_2O_3.

Compound	Gd_2O_3	Tb_2O_3	Dy_2O_3	Er_2O_3	Tm_2O_3	Yb_2O_3	Lu_2O_3
O 1s BE ±0.2 (eV)	527.9	527.4	528.7	528.9	527.9	527.9	528.0
O 2p BE ±0.2 (eV)	4.0	3.5	4.8	5.0	4.0	4.0	4.1

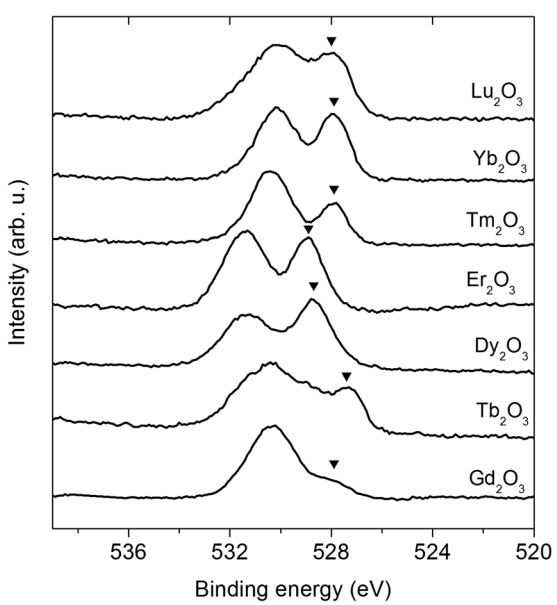

FIG. 2. X-ray photoelectron spectra of O 1s core region of Ln_2O_3 (Ln = Gd, Tb, Dy, Er, Tm, Yb, Lu).

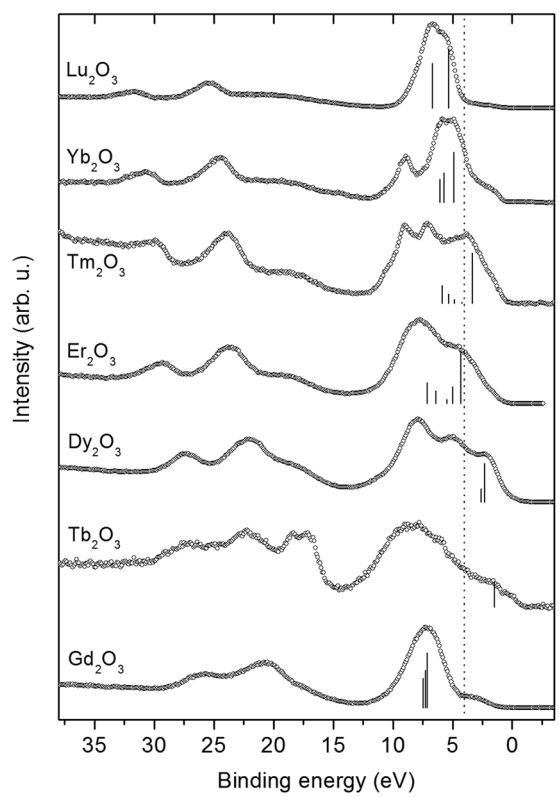

FIG. 3. X-ray photoelectron spectra of the XPS VB (valence band) of Ln_2O_3 (Ln = Gd, Tb, Dy, Er, Tm, Yb, Lu).

Lu $4f_{7/2}$ lowest BE is located at 5.9 eV. The shoulder at lower BE is due to O 2p state. For Yb_2O_3, the three bars of the lowest BEs and the more significant intensities are represented, corresponding to transitions to the $^3H_6$, $^3F_4$, and $^3H_5$ final states of Yb^{4+} in the order of increasing BE. The Lu $4f_{7/2}$ lowest BE is located at 4.9 eV. The five lowest BEs and more significantly intense peaks ($^5I_8$, $^5I_7$, $^5I_6$, $^5F_5$, and $^5G_6$ final states of Er^{4+} in the order of increasing energy) were used to fit the lower BE side of the 4f multiplet of Er_2O_3. The Lu $4f_{7/2}$ lowest BE is located at 4.3 eV. For Dy_2O_3, the first two multiplet bands were used ($^7F_6$ and $^7F_5$ in the order of increasing energy). The Lu $4f_{7/2}$ lowest BE is located 2.3 eV. Figure 3 presents the fit of the 4f peaks for Gd_2O_3, from the first four ^7F_J (J = 0, 1, 2, 3) final state levels with a significant intensity. The Gd $4f_{7/2}$ lowest BE is located at 7.1 eV. The shoulder at lower BE can be attributed to the O 2p states. For Tb_2O_3 the first band corresponds to $^8S_{7/2}$ final state transition. The Tb $4f_{7/2}$ lowest BE is therefore found at 1.5 eV. For Tm_2O_3, the lowest energy bands with significant intensity ($^4I_{15/2}$, $^4I_{13/2}$, $^4I_{11/2}$, $^4F_{9/2}$, and $^2H_{11/2}$) were used to fit the spectrum. The Lu $4f_{7/2}$ lowest BE was found at 3.3 eV.

All these values are reported in Table II. The energy differences between the O 2p and the Ln 4f states were calculated in Table II. We consider that they represent the position of the $4f^n$ Ln^{3+} state relative to the top of the valence band according to this work. They were displayed as red circles in the energy diagram of Fig. 4. The top of the valence band is defined as the zero of energy. Error bars are drawn in Fig. 4 relatively to the uncertainty of the O 1s position. These error bars were evaluated as ± 0.4 eV as the error in locating on the one hand O1s peaks and on the other hand Ln $4f_{7/2}$ peaks is 0.2 eV each.

B. Energy levels diagrams of trivalent lanthanides

1. The three-parameters model

Using a three-parameter model developed by Dorenbos, a predictive energy level scheme of trivalent lanthanides in $(Lu_{0.5}Gd_{0.5})_2O_3$ was constructed and shown as "model" curves in Fig. 4. The notation presented by Dorenbos[18] is also used in the present paper. Levels energies E^X (n, Q, A) are expressed as a function of the number of electrons n in the $4f^n5d^0$ fundamental configuration of the lanthanide, its ionic charge Q and the type of compound A. Superscript X indicates the type of considered transition. For instance E^{Vf} (6, 3 + , Lu_2O_3) is the energy difference between the top of the valence band (V) and the $4f^6$ ground state of Eu^{3+} whereas E^{CT}(0, 4+, Lu_2O_3) represents the energy of the charge transfer state (superscript CT) of Ce^{4+} (n = 0) in Lu_2O_3. In Fig. 4 the zero of energy was taken as the top of the valence band by convention.

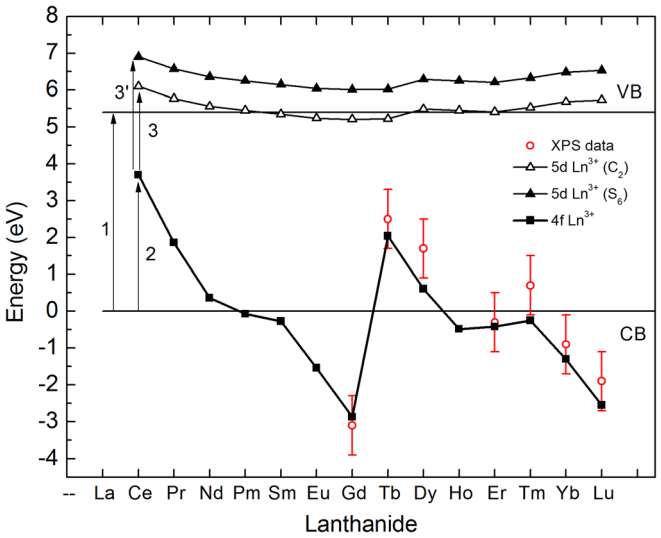

FIG. 4. (Color online) Energy level diagram of Ln^{3+} 4f and 5d states in $(Lu_{0.5}Gd_{0.5})_2O_3$ according to XPS data and model.

The energy scheme of Fig. 4 was first built from the experimental knowledge of:

(i) The bandgap $E^{VC}[(Lu_{0.5}Gd_{0.5})_2O_3]$ between the top of the valence band (VB) and the bottom of the conduction band (CB). E_{VC} corresponds to the creation of a free electron in the conduction band and a free hole in the valence band.

(ii) The Ce^{4+} charge transfer energy E^{CT}(0, 4+, $(Lu_{0.5}Gd_{0.5})_2O_3$).

(iii) The Ce^{3+} $4f^n \rightarrow 4f^{n-1}5d^1$ transition energy E^{fd} (1, 3+, $(Lu_{0.5}Gd_{0.5})_2O_3$).

a. Parameter (i), location of the bands. The bandgap of $(Lu_{0.5}Gd_{0.5})_2O_3$ was determined by measuring the reflectance spectrum of a $(Lu_{0.5}Gd_{0.5})_2O_3$ powder shown in Fig. 5 as curve (a). The Kubelka-Munk function F(R)[33] expresses the absorbed fraction of light α from the scattered fraction of light R and α was then calculated as $\alpha = F(R) = (1-R)^2/2R$, where R is the reflectance shown in Fig. 5(a). The Tauc law[35,36] was then used to obtain the fundamental absorption edge by considering that $\alpha(h\nu) = \text{constant} \times (h\nu - E_G)^n/h\nu$ where α is the absorption, hν the radiation energy and E_G the optical bandgap. n depends on the type of gap (direct or indirect). $(Lu_{0.5}Gd_{0.5})_2O_3$ having a very similar structure to Y_2O_3 we assume that similarly to Y_2O_3, $(Lu_{0.5}Gd_{0.5})_2O_3$ presents a direct bandgap and therefore $n = [1/2]$ $(\alpha \times h\nu)^2$ was drawn in the inset of Fig. 5 in order to determine E_{VC} on the figure. The value of 5.4 eV was found and was reported in the scheme Fig. 4 as the difference between the top of the valence band and the bottom of the conduction band (arrow 1).

TABLE II. Ln 4f binding energies (BEs) referred to O 2p peak located at 4.0 eV in Ln_2O_3. ΔBE is the energy difference between the top of the valence band and the $4f_{7/2}$ lowest BE of the multiplet.

Compound	Gd_2O_3	Tb_2O_3	Dy_2O_3	Er_2O_3	Tm_2O_3	Yb_2O_3	Lu_2O_3
Ln $4f_{7/2}$ BE ±0.2 (eV)	7.1	1.5	2.3	4.3	3.3	4.9	5.9
ΔBE = O 2p BE-Ln 4f BE ±0.4 (eV)	-3.1	+2.5	+1.7	-0.3	+0.7	-0.9	-1.9

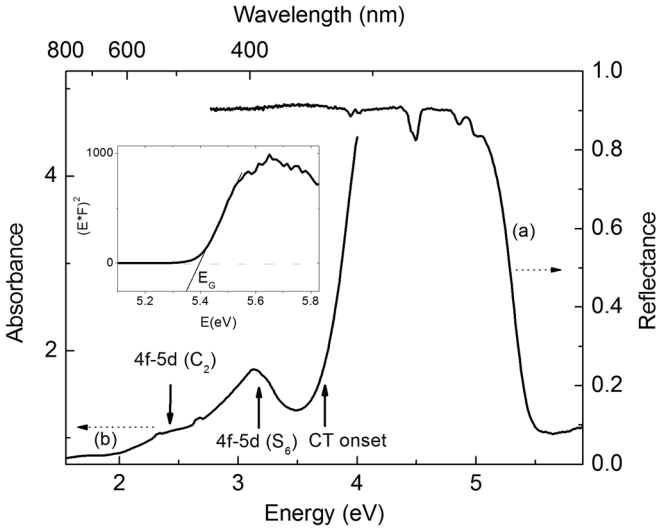

FIG. 5. (a) Reflectance spectrum of $(Lu_{0.5}Gd_{0.5})_2O_3$ powder, (b) absorbance spectra of $(Lu_{0.5}Gd_{0.5})_2O_3$: Ce^{3+}/Ce^{4+} ceramics. Inset: Kubelka-Munk function of the reflectance spectrum of $(Lu_{0.5}Gd_{0.5})_2O_3$.

b. Parameter (ii), location of the 4f^n ground states. In order to determine the charge transfer energy from oxygen to Ce^{4+} in $(Lu_{0.5}Gd_{0.5})_2O_3$, the transmission spectrum of $(Lu_{0.5}Gd_{0.5})_2O_3$: Ce^{3+}/Ce^{4+} ceramics with nominal Ce concentration of 1000 ppm was measured. The ceramics was prepared in air so that cerium is present in both 3 + and 4 + oxidation states. The resulting absorbance is shown in Fig. 5(b). The introduction of cerium results on the one hand in two moderate absorption bands peaking at 2.4 and 3.2 eV, corresponding to 4f-5d absorption transitions of Ce^{3+}, and on the other hand in a strong absorption band at 4.1 eV attributed to CT transition from oxygen to Ce^{4+} ions. Following arguments given in Ref. 18, the charge transfer energy obtained as the onset (at 3.7 eV) of the charge transfer band is taken as the difference between the top of the valence band and Ce^{3+} fundamental level and represented by arrow 2 in Fig. 4. From this "anchor" point, the location of the other trivalent lanthanides 4f ground states is inferred by Dorenbos model.[19] It is represented by black filled squares in Fig. 4.

c. Parameter (iii), location of the 4f^{n-1}5d excited states. The two 4f-5d transitions at 2.4 and 3.2 eV were attributed to Ce^{3+} in, respectively, C_2 (arrow 3) and S_6 (arrow 3′) sites.[37,38] The location of the other lanthanides 5d levels does not vary much relative to the Ce^{3+} 5d position. It is represented as black triangles in Fig. 4 as described by Dorenbos.[18]

C. Agreement between experiments and 3-parameters model

The location of Gd^{3+}, Tb^{3+}, Er^{3+}, Yb^{3+}, Lu^{3+}, Dy^{3+}, and Tm^{3+} as determined by XPS analysis were found consistent with Dorenbos model within the XPS (±0.4 eV) and model (0.5 eV) error bars. In a previous work by Pidol *et al.*,[39] Er^{3+}, Yb^{3+}, and Lu^{3+} levels determined by XPS and located within the valence band, were found lower by around 1 eV than the model, whereas Ce^{3+} level located inside the bandgap was found by XPS at the same position as found by the model. Data on $(Lu_{0.5}Gd_{0.5})_2O_3$ appear trustful since many lanthanide ions were considered and data were handled with care.

Let us note that no influence of final state effect seem to have contributed more than the experimental error bar. By making the assumption of the frozen orbital approximation, i.e., the system, initially possessing n electrons, gets ionized after x-ray irradiation to become a "frozen" n-1 electrons system, identical to the initial n electrons system, the binding energy was simply deduced from the measured kinetic energy of the photoelectrons by the formula: $E_b = E_X - E_k$ where E_b is the binding energy, E_X the incident x-ray energy, and E_k the measured kinetic energy of the photoelectron. However, the frozen orbital approximation is not exact as a large relaxation of the n-1 electrons system takes place after ionization: the hole left on the atom polarizes its environment and lowers the kinetic energy of the ejected photoelectron. In a first approximation this lowering is large but similar for any photoelectron, and therefore, taken as a systematic shift in binding energies. Looking into fine contributions, however, one should take into account this final state effect (polarization energy). Poole *et al.*[40] calculated polarization energies at both M^{2+} (M = Ca, Sr, Ba) and F^- sites in alkaline-earth fluorides and showed that they were different for the cation and the anion sites. Therefore, they calculated a correction in the binding energy differences between M^{2+} and F^- states of 0.33, 0.45, and 0.63 eV in, respectively, CaF_2, SrF_2, and BaF_2. However, the F^- anion is more polarizable than the oxygen ion and a much larger difference in bond strength exists along this alkaline earth fluorides series than in the Ln_2O_3 series. Based on these arguments, we believe that the effect of polarization energy on our results should be smaller than the ones on the alkaline earth series and therefore smaller or at most in the order or the error bar of the XPS data.

By considering Tb^{3+}, Dy^{3+}, Tm^{3+}, Yb^{3+}, and Lu^{3+}, one may think that the model systematically and slightly underevaluates the energy position of Ln^{3+}. This is possibly due to the underestimation of the charge transfer band position as it is determined by optical absorption. XPS data suggest that the actual position of all Ln^{3+} levels in $(Lu_{0.5}Gd_{0.5})_2O_3$ may actually be 0.5 eV higher than represented by the model in Fig. 4.

The diagram of Fig. 4 shows that the lowest 5d levels of all the trivalent lanthanides are located inside the conduction band or very close to its bottom. When $4f^n - 4f^{n-1}5d^1$ transitions are excited, photoionization therefore readily happens. This explains why we could not observe any 5d-4f Ce^{3+} luminescence in $(Lu_{0.5}Gd_{0.5})_2O_3$:Ce. While the $(Lu_{0.5}Gd_{0.5})_2O_3$ host is very interesting in scintillation, Ce^{3+} can unfortunately not be chosen as the luminescent ion. F-f Eu^{3+} luminescence though much slower than Ce^{3+} 5d-4f luminescence is better adapted to $(Lu_{0.5}Gd_{0.5})_2O_3$ host. The situation appears very similar to Lu_2O_3 where Ce^{3+} 5d-4f luminescence has never been observed in normal conditions.[37] Shen *et al.*[41] observed that a high pressure applied on Lu_2O_3:Ce^{3+} crystals enables to observe a luminescence at 610 nm attributed to Ce^{3+} 5d-4f luminescence as pressure induced an electronic crossover of the excited Ce (5d) state and conduction band edge. The same might be observable in $(Lu_{0.5}Gd_{0.5})_2O_3$:Ce.

IV. CONCLUSION

Mixed lutetium gadolinium sesquioxide is a material of choice in scintillation since as for Lu_2O_3 the material is very dense. However, this study confirmed that no Ce^{3+} 5d-4f emission could be obtained from Ce^{3+} doping due to the position of the dopant levels relative to the crystal host bands. More generally, we discussed the location of the energy levels of all the trivalent lanthanides in $(Lu_{0.5}Gd_{0.5})_2O_3$. We carried out an XPS study of several heavy lanthanides Ln_2O_3 (Ln = Gd, Tb, Dy, Er, Tm, Yb, Lu). By carefully examining the position of the lanthanide 4f peaks and the oxygen 1s and 2p peaks in the lanthanides sesquioxides as well as in Sc_2O_3 and Y_2O_3 we proposed a location of the Ln^{3+} ground states relative to the top of the valence band of $(Lu_{0.5}Gd_{0.5})_2O_3$ within an error bar of ± 0.4 eV. The results were compared to optical data and predictions. The location by XPS of the ground states of Ln^{3+} was found consistent with Dorenbos predictions within the error bars of model and XPS measurements. However for the majority of Ln^{3+} a slight underestimation of the Ln^{3+} energy position by the model was noticed. This was attributed to an underestimating measurement of Ce^{4+} charge transfer band in $(Lu_{0.5}Gd_{0.5})_2O_3$. When carried out with care XPS measurements offer a valuable complementing tool to adjust the model predictions of Ln^{3+} energy levels based on optical absorption. More studies should be conducted to confirm any systematic difference between model (based on optical absorption) and XPS data.

ACKNOWLEDGEMENTS

This work was supported by Saint-Gobain Crystals.

[1]P. Dorenbos, J. Lum. **91**, 91 (2000).
[2]P. Dorenbos, J. Lum. **87-89**, 970 (2000).
[3]P. Dorenbos, J. Lum. **91**, 155 (2000).
[4]P. Dorenbos, J. Phys.: Condens. Matter **15**, 575 (2003).
[5]C. Dujardin, C. Pedrini, J. C. Gâcon, A. G. Petrosyan, A. N. Belsky, and A. N. Vasil'ev, J. Phys.: Condens. Matter **9**, 5229 (1997).
[6]A. Bessière, P. Dorenbos, C. W. E. van Eijk, E. Yamagishi, C. Hidaka, and T. Takisawa, J. Electrochem. Soc. **151**(12), 254 (2004).
[7]D. S. Hamilton, S. K. Gayen, G. J. Pogatshnik, and R. D. Shen, Phys. Rev. B **39**, 8807 (1989).
[8]A. Bessière, P. Dorenbos, C. W. E. van Eijk, K.W. Krämer, H. U. Güdel, C. de Mello Donega, and A. Meijerink, Nucl. Instr. Meth. Phys. Res. A **53**, 22 (2005).
[9]L. Pidol, B. Viana, A. Bessière, A. Galtayries, P. Dorenbos, and B. Ferrand, Mat. Sci. Forum **555**, 371 (2007).
[10]D. Pauwels, N. Le Masson, B. Viana, A. Kahn-Harari, E. V. D. van Loef, P. Dorenbos, and C. W. E. van Eijk, IEEE Trans. Nucl. Sci. **47**(6), 1787 (2000).
[11]L. Pidol, A. Kahn-Harari, B. Viana, E. Virey, B. Ferrand, P. Dorenbos, J. T. M de Haas, and C. W. E. van Eijk, IEEE Trans. Nucl. Sci. **51**(3), 1084 (2004).
[12]A. Lecointre, A. Bessière, A. J. J. Bos, P. Dorenbos, B. Viana, and S. Jacquart, J. Phys. Chem. C **115**, 4217 (2011).
[13]A. J. J. Bos, P. Dorenbos, A. Bessière, A. Lecointre, M. Bedu, M. Bettinelli, and F. Piccinelli, "Study of TL glowcurves of YPO_4 double doped with lanthanide ions," Rad. Measur. (2011) (in press).
[14]A. Lecointre, A. Bessière, B. Viana, and D. Gourier, Rad. Meas. **45**, 497 (2010).
[15]P. Dorenbos, L. Pierron, L. Dinca, C. W. E. van Eijk, A. Kahn-Harari, and B. Viana, J. Phys. Cond. Matter **15**(3), 511 (2003).
[16]A. Sidorenko, P. Dorenbos, C. W. E. van Eijk, A. J. J. Bos, and P. A. Rodnyi, Nucl. Instrum. Meth. A **537**, 81 (2005).
[17]P. Dorenbos, J. Phys.: Condens. Matter **15**, 2645 (2003).
[18]P. Dorenbos, J. Phys.: Condens. Matter **15**, 8417 (2003).
[19]P. Dorenbos, A. H. Krumpel, E. van der Kolk, P. Boutinaud, M. Bettinelli, and E. Cavalli, Opt. Mater. **32**(12), 1681 (2010).
[20]P. Dorenbos, J. Phys.: Condens. Matter **15**, 6249 (2003).
[21]C. W. Thiel, H. Cruguel, H. Wu, Y. Sun, G. J. Lapeyre, R. L. Cone, R. W. Equall, and R. M. Macfarlane, Phys. Rev. B **64**, 08510 (2001).
[22]C. W. Thiel and R. L. Cone, J. Lum. **131**, 386 (2011).
[23]L. Pidol, B. Viana, A. Kahn-Harari, A. Galtayries, A. Bessière, and P. Dorenbos, J. Appl. Phys. **95**(12), 7731 (2004).
[24]A. Bessière, P. Dorenbos, C. W. E. van Eijk, K. W. Krämer, H. U. Güdel, and A. Galtayries, J. Lum. **117**, 187 (2006).
[25]E. Zych and J. Trojan-Piegza, J. Lum. **122-123**, 335 (2007).
[26]H. Rétot, S. Blahuta, A. Bessière, B. Viana, B. LaCourse, and E. Mattman, J. Phys. D: Appl. Phys. **44**, 235101 (2011).
[27]Y.-N. Xu, Z. Gu, and W. Y. Ching, Phys. Rev. B **56**, 14993 (1997).
[28]D. Bouttet, C. Dujardin, C. Pedrini, W. Brunat, D. Tran Minh Duc, and J. Y. Gesland, *Proc. Int. Conf. on Inorganic Scintillators and Their Applications SCINT95* (Delft University Press, The Netherlands, 1996).
[29]M. Cardona and L. Ley, *Photoemission in Solids I: General Principles* (Springer-Verlag, Berlin, 1978).
[30]M. Perego, G. Seguini, G. Scarel, and M. Fanciulli, Surf. Interf. Anal. **38**, 494 (2006).
[31]A. Ubaldini and M. M. Carnasciali, J. All. Comp. **454**, 374 (2008).
[32]R. D. Shannon, Acta Crystallogr. A **32**, 751 (1976).
[33]G. Körtum, *Reflectance Spectroscopy: Principles, Methods, Applications* (Springer, Berlin, 1969), p. 111.
[34]P. A. Cox, *Structure and Bonding*, edited by J. D. Dunitz (Springer-Verlag, Berlin, 1975), Vol. 24, pp. 59–81.
[35]S. Sirohi and T. P. Sharma, Opt. Mater. **13**, 267 (1999).
[36]N. F. Mott and E. A. Davis, *Electronic Processes in Non-Crystalline Materials* (Clarendon Press, Oxford, 1979).
[37]M. Raukas, S. A. Basun, W. van Schaik, W. M. Yen, and U. Happek, Appl. Phys. Lett. **69**, 3300 (1996).
[38]G. A. Slack, S. L. Dole, V. Tsoukala, and G. S. Nolas, J. Opt. Soc. Am. B **11**, 961 (1994).
[39]L. Pidol, B. Viana, A. Galtayries, and P. Dorenbos, Phys. Rev. B **72**, 125 (2005).
[40]R. T. Poole, J. Szajman, R. C. G. Leckey, J. G. Jenkin, and J. Liesegang, Phys. Rev. B **12**, 5872 (1976).
[41]Y. Shen, D. B. Gatch, U. R. R. Mendoza, G. Cunningham, R. S. Meltzer, W. M. Yen, and K. L. Bray, Phys. Rev. B **65**, 212103 (2002).